J Membrane Biol (2008) 222:127–139
DOI 10.1007/s00232-008-9106-8

Atomic Force Microscopy Imaging of *Bacillus thuringiensis* Cry1 Toxins Interacting with Insect Midgut Apical Membranes

Eric Laflamme · Antonella Badia · Michel Lafleur · Jean-Louis Schwartz · Raynald Laprade

Received: 14 December 2007 / Accepted: 23 March 2008 / Published online: 4 June 2008

Abstract Atomic force microscopy was used to image *Bacillus thuringiensis* (*Bt*) toxins interacting with their natural targets, *Manduca sexta* midgut brush border membranes (BBMs), as well as with dipalmitoylphosphatidylcholine-dioleoylphosphatidylcholine (DPPC-DOPC) solid-supported lipid bilayers. In lipid bilayers, Cry1Aa formed structures 30–60 nm wide and 3–7 nm high, mostly at the interface of domains formed by the two different lipids or at the edge of DOPC-enriched domains. BBM vesicles, in the absence of toxin, formed flat membrane fragments of up to 25 μm^2 and 4.2 nm high, with irregular embedded structures. After incubation with Cry1Aa, Cry1Ac and Cry1C, which are active against *M. sexta*, new structures, 35 nm wide and 5.1–6.7 nm high, were observed in some membrane fragments, sometimes only in particular regions. Their density, which reached a plateau within 4 h, was toxin- and concentration-dependent. The structures formed by Cry1Ac were often grouped into dense, two-dimensional arrangements. No such specific interactions were observed with Cry1Ba, which is inactive against *M. sexta*. This study provides the first visual demonstration of specific interactions of *Bt* toxins with insect midgut BBMs at the nanometric scale. The observed structures likely represent the protein complexes forming functional *Bt* pores in target membranes.

E. Laflamme · M. Lafleur · J.-L. Schwartz · R. Laprade (✉)
GÉPROM, Université de Montréal, Centre ville station,
PO Box 6128, Quebec, Montreal, Canada H3C 3J7
e-mail: raynald.laprade@umontreal.ca

A. Badia · M. Lafleur
Département de Chimie, Université de Montréal, Centre ville station, PO Box 6128, Quebec, Montreal, Canada H3C 3J7

Keywords Brush border membrane · Cry1Aa · Cry1Ac · Cry1C · Target membrane · *Manduca sexta*

Introduction

Delta endotoxins from *Bacillus thuringiensis* (*Bt*) are presently the most widely used biological insecticides (Schnepf et al. 1998; Whalon and Wingerd 2003). Following ingestion by the larvae, solubilization in the gut and activation by intestinal proteases, the toxin binds to receptors at the apical membrane of the midgut epithelium and inserts into the membrane to form pores that abolish transmembrane ionic and electrical gradients, leading to cell death (Knowles and Ellar 1987). However, several details of the mode of action of *Bt* toxins remain largely unknown, in particular the oligomerization step that leads to the formation of functional pores in the membrane. Structural models have been proposed in which several toxin molecules come together to form a pore (Hodgman and Ellar 1990; Gill et al. 1992), and the first spatial arrangement of domain-I helices of Cry1Aa toxin in lipid bilayers was suggested (Schwartz et al. 1997a) and, subsequently, refined (Masson et al. 1999). These oligomeric models were based on X-ray crystallographic data of the three-domain Cry3Aa and Cry1Aa toxins (Li, Carroll and Ellar 1991; Grochulski et al. 1995). However, the actual arrangement of the toxin molecules in artificial lipid bilayers with or without receptors, in native apical membranes or in vivo may be quite different. Furthermore, recent studies suggest a two-step insertion process in which an oligomeric prepore is formed first, when several toxins bind to cadherin receptors anchored to the membrane by a single transmembrane segment. In the second step, functional membrane pores are formed in lipid rafts, following

the binding of the prepore complexes to aminopeptidase N (APN) receptors attached to the rafts by their glycosylphosphatidylinositol (GPI) tails (Zhuang et al. 2002; Bravo et al. 2004).

Atomic force microscopy (AFM) is a recent, powerful tool that allows the imaging of various types of materials at the nanometric scale, including soft biological samples (reviewed in El Kirat et al. 2005). Indeed, lipid bilayers, natural membranes as well as proteins have been imaged by AFM. In addition, lateral resolution of up to 0.5 nm could be obtained with proteins forming regular two-dimensional arrays (Müller et al. 2000). Several experimental approaches have been used, such as patch-clamp pipette excision to isolate and image membranes and protein complexes (Danker et al. 1997), serial thin-sectioning of single cells to reveal their inner ultrastructure (Chen et al. 2005) and isolation of disc membranes by centrifugation to investigate the organization of the G protein–coupled rhodopsin receptor in the native membrane (Fotiadis et al. 2004). Of particular interest to the area of *Bt* toxin assembly characterization, Cry1Aa, a *Bt* toxin active against caterpillars, and Cry4Ba, a *Bt* toxin that kills mosquito larvae, have been visualized by AFM after being inserted into supported purified or synthetic lipid monolayers or bilayers (Vié et al. 2001; Puntheeranurak et al. 2005). While there is presently no information on how many toxin molecules form the pores and whether receptor proteins participate in their architecture, the toxins appeared to associate and form tetrameric structures (Vié et al. 2001), supporting the four-subunit model proposed earlier for the *Bt* pore (Schwartz et al. 1997a; Masson et al. 1999).

These previous AFM studies implicated nonspecific interactions between *Bt* toxins and purified or synthetic lipids. In order to address the specificity of these toxins to their target membranes and to elucidate further the structures they form in these membranes in their aqueous environment, AFM was used to image these proteins in the presence of the midgut brush border membrane (BBM) from tobacco hornworm larvae (*Manduca sexta*, Lepidoptera). Three related Cry1 toxins (Cry1Aa, Cry1Ac and Cry1C), all active against *M. sexta* larvae and sharing at least 67% amino acid identity (Höfte and Whiteley 1989), were used for these studies, as well as Cry1Ba (55–58% or more identity with the former) to which the larvae are not sensitive (Höfte et al. 1988; Van Rie et al. 1989). For comparison, the insertion of Cry1Aa into supported dipalmitoylphosphatidylcholine-dioleoylphosphatidylcholine (DPPC-DOPC) bilayers formed by liposome deposition on mica was also investigated. This work provides the first visual demonstration at the nanometric scale of the interaction between *Bt* toxins and their target native membranes under pseudophysiological conditions. It shows that the toxins form structures approximately 35 nm in diameter and 5.1–6.7 nm in height and that the distribution and organization of these structures vary depending on the toxin. These differences are likely related to specific protein–protein interactions, whereas no such interactions were observed with Cry1Ba, which is not toxic to the target insect.

Materials and Methods

Chemicals

DPPC and DOPC were purchased from Avanti Polar Lipids (Alabaster, AL) and phospholipase A_2 (PLA_2), from honeybee venom (P9279), was obtained from Sigma-Aldrich (Oakville, Canada).

Toxins

Cry1Aa, Cry1Ac, Cry1C and Cry1B toxins were obtained from *Bt* strains producing the appropriate single recombinant toxins. The toxins were solubilized, trypsin-activated and purified by fast protein liquid chromatography as described elsewhere (Masson et al. 1989, 1994). Stock solutions were prepared in 25 mM Tris-HCl (pH 9.4) at a concentration of 2 mg/ml and kept at 4°C. They were diluted to the appropriate concentrations in 10 mM HEPES-KOH, pH 7.5, the normal experimental solution (NES).

BBM Vesicles

Whole midguts were isolated from fifth-instar *M. sexta* larvae (Department of Entomology Insectary, North Carolina State University, Raleigh, NC), freed of attached malpighian tubules and cleared of their contents. They were rinsed thoroughly with ice-cold 300 mM sucrose, 17 mM Tris-HCl (pH 7.5) and 5 mM EGTA and stored at −80°C until use. BBM vesicles (BBMVs) were prepared using a magnesium precipitation and differential centrifugation technique (Wolfersberger et al. 1987). The final membrane preparation was resuspended in NES at a final stock suspension concentration of 0.5 mg/ml of protein and stored at −80°C until use.

Formation of Supported DPPC/DOPC Bilayers and Deposition of BBMs

Multilamellar liposomes were prepared from stock solutions of DOPC and DPPC in chloroform (1 mg/ml). Two milliliters of a 1:1 mixture (v/v) of DPPC/DOPC were

dried under nitrogen and left under vacuum for at least 16 h. The lipids were reconstituted in 2 ml diluted phosphate-buffered saline (dPBS) containing 2.5 mM Na_2HPO_4, 16.7 mM NaCl (pH 7.4), to a final concentration of 1 mg/ml. Small liposomes were prepared by sonication at 60°C for 12 min. For Cry1Aa toxin–enriched liposomes, 5–50 μg/ml of toxin was added to the liposome suspension immediately after sonication, after which the suspension was vortexed for 1 min and allowed to settle for 30 min. Pure liposomes or toxin-enriched liposomes were then deposited on freshly cleaved mica and incubated at 60°C for 2 h to form, through liposome fusion, a supported bilayer, which was then rinsed with dPBS to make it ready for imaging.

For BBM deposition, a BBMV stock suspension was diluted in NES to a final concentration of 25 μg/ml protein (final volume 400 μl), incubated overnight on mica at room temperature and rinsed with NES prior to imaging. Overnight incubation significantly increased the probability of finding membrane fragments on the mica surface and proved practical given the long duration of the experiments due to the time required to locate the membrane fragments and image them first in the absence of toxin, and then, in its presence, for as much as four hours.

AFM Imaging

AFM imaging was performed at room temperature in the magnetic alternating current (MAC) mode using a PicoSPM microscope (Molecular Imaging, Tempe, AZ) equipped with a 30-μm scanner and a fluid cell. AFM tips (MAC levers T1, Molecular Imaging) with nominal spring constants of either 0.95 or 0.6 N/m were used. The cantilever frequency was between 20 and 60 kHz and the scanning rate between 1.15 and 2.0 Hz. Except for toxin-enriched liposome preparations, imaging was always performed before addition of the toxin, either with the supported bilayer or with BBMs alone. After withdrawing the AFM tip by 5 μm and turning off the drive of the MAC mode controller, toxin (500 μl of either 8 or 40 μg/ml toxin in NES) was added in the fluid cell through a solution exchange system made of a small polyethylene tube (0.86 mm inside diameter) and a 1-ml syringe, and the same area of the BBM sample was imaged. Each sample was incubated with either 8 or 40 μg/ml of toxin for 1 and 4 h and, in some experiments, for 2 h. After each incubation period, the preparation was rinsed with NES and the same observation area was imaged in this solution for variable periods of time (20–120 min). Each experimental condition was repeated at least 10 times. Given the intrinsic size overestimation by the AFM tip in the horizontal plane (Markiewicz and Goh 1994), the diameter of the observed structures was defined as their width at half-height. Measurements are given as means ± standard error of the mean (SEM).

Results and Discussion

Imaging of Cry1Aa Toxin on DPPC-DOPC Bilayers

The interaction of Cry1Aa toxin with a DPPC-DOPC (1:1 v/v) bilayer deposited on mica by liposome fusion was investigated (Milhiet et al. 2001). In the absence of toxin, the substrate was almost completely covered by the bilayer. Figure 1A shows a typical image where three height levels are observed corresponding to bare mica (dark brown), fluid-phase DOPC-enriched (light brown) and gel/solid-phase DPPC-enriched (yellow-brown) domains. The bilayer consisted, at room temperature, of DPPC-enriched domains in the gel phase surrounded by DOPC-enriched matrix in the fluid phase, as evidenced by the difference of their measured thicknesses above the mica surface (5.6 ± 0.3 nm [$n = 8$] vs. 4.2 ± 0.2 nm [$n = 8$], respectively) (Fig. 1A). DPPC-enriched domains represented about 22%, DOPC-enriched ones 72% and mica 6% of the total surface, consistent with other observations of mixtures of gel and fluid phase lipids (Milhiet et al. 2006; Rinia et al. 2001). After a 2-h incubation of the DPPC-DOPC bilayer with Cry1Aa, either at room temperature or at 55°C to promote toxin incorporation, no structural changes were observed. With toxin-enriched liposomes, bilayer coverage of the mica surface was only partial (Fig. 1B) and appeared to be inversely related to toxin concentration (not shown), likely due to preferential interaction of the toxin with the DOPC-enriched fluid phase and consequent interference with the fusion process. Indeed, in the typical image shown in Fig. 1B, at a toxin dose of 40 μg/ml, DPPC-enriched domains covered about 33%, DOPC-enriched domains 27% and mica 40% of the total image area. However, in this case, a few isolated structures of about 30×60 nm with heights varying 3–7 nm were observed protruding from the bilayer surface, mostly at the interface of the DPPC-DOPC regions as well as at the periphery of DOPC domains alone (Fig. 1B). As shown in Fig. 1C–E, these structures appear to be composed of smaller substructures, as demonstrated by the vertical profile lines shown below the AFM images. These assemblies may represent oligomers of several toxin molecules.

Previous studies (Schwartz et al. 1993; Peyronnet et al. 2002) have shown that Cry1 toxins insert into lipid bilayers and form pores in the absence of *Bt* receptors. Of particular interest to the present study is the first attempt to visualize the architecture of the pores formed by Cry1Aa toxin in a lipid bilayer environment using AFM imaging (Vié et al. 2001). The images showed toxin aggregates of 30–100 nm

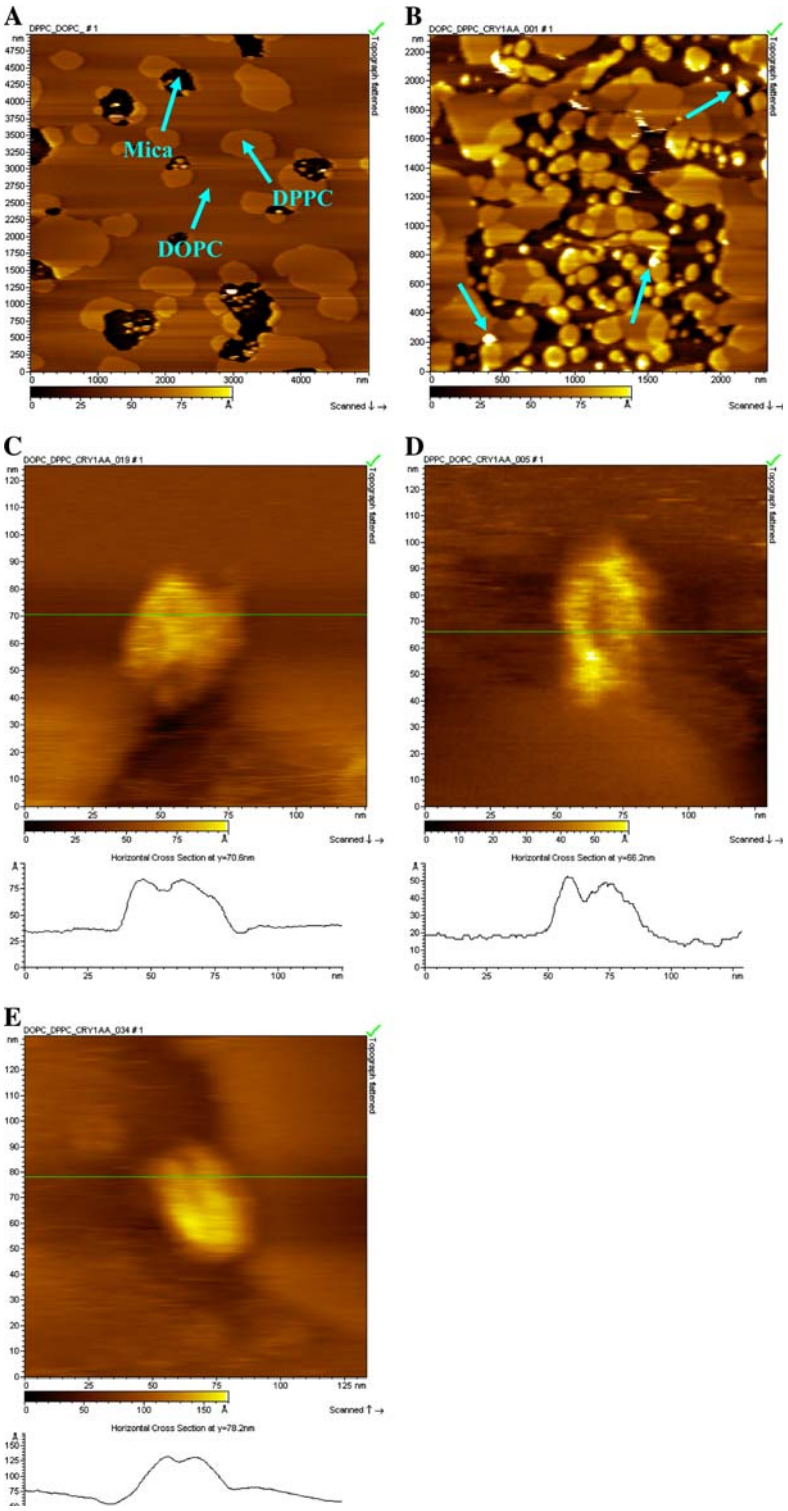

Fig. 1 AFM imaging of a typical DPPC-DOPC (1:1 v/v) supported bilayer on mica prepared by liposome fusion. (**A**) In the absence of toxin, DPPC domains occupy about 22%, DOPC 72% and mica 6% of the total image area. (**B**) With Cry1Aa toxin–preloaded liposomes (40 μg/ml toxin), DPPC covers about 33%, DOPC 27% and mica 40% of the total image area. Imaging was performed 2 h following toxin-enriched liposome deposition on the mica surface at 60°C. *Arrows* point to structures formed by Cry1Aa (these are never observed in the absence of toxin). (**C–E**) Similar structures observed in independently acquired images recorded under identical conditions and magnified further ×20. These structures measure approximately 30 × 60 nm, with heights varying 3–7 nm. *Horizontal bars* below the images represent the color-coded heights on the images. *Vertical profiles along the green lines* are given below the images

in diameter. In addition, substructures could be resolved, primarily at the periphery of these aggregates, suggesting a tetrameric arrangement with a central depression of 1.5 nm in diameter and with a large part of the toxin molecules likely embedded in the bilayer. In the latter study, the toxin was first allowed to insert into a monolayer at the air/water interface, followed by deposition of the latter onto a second monolayer supported on mica. This insertion process was different from the actual mechanism in which the toxin partitions into a free-standing bilayer membrane directly from the aqueous phase. In the only other AFM study with *Bt* Cry toxins, Cry4Ba was found to form, in supported

bilayers, structures of 20–30 nm in cross section and 2–4 nm high that were preferentially localized along the edges of membrane defects (Puntheeranurak et al. 2005). In the latter study as well as the present one, substructures at the nanometric scale resolution could not be observed. This limited resolution may be linked to the particular geometry of these protein molecules over and into the lipids. Limited resolution may also be a characteristic of imaging isolated proteins as inspection of the recent literature strongly suggests that extended two-dimensional (2-D) arrays or closely packed arrangements are a prerequisite for high-resolution AFM imaging of membrane proteins (Janovjak et al. 2006).

Imaging of BBMs from *M. sexta* Midgut

To mimic the biological situation, we imaged *M. sexta* midgut BBMs. These membranes contain the receptors that bind *Bt* toxins and promote pore formation (Schnepf et al. 1998). We used the same BBM preparation under the same environmental conditions as used in our osmotic swelling permeabilization assays (Fortier et al. 2007). After incubation with the BBMV solution, the mica was mostly covered by irregularly dispersed bumps of heights varying from a few to hundreds of nanometers, which could possibly represent unfused vesicles (Wielert-Badt et al. 2002) or protein aggregates after membrane remodeling, namely, lateral segregation of lipids in a fluid phase (Fig. 2). From time to time, larger flat areas were also seen (one to two regions on a scanned surface of 250 μm^2), with a surface area ranging 1–25 μm^2 and a height of 4.2 ± 0.1 nm ($n = 15$) (Fig. 2). Moreover, thicker flat domains of 5.1 ± 0.1 nm in height ($n = 8$) and up to 1 μm^2, indicative of lipid phase separation, were also detected within these flat areas (Fig. 3). Interestingly, this difference in thickness of about 1 nm between thinner and thicker regions of the bilayer is identical to that observed on synthetic lipid mixtures of phosphatidylcholine with sphingolipids and cholesterol, mimicking biological membrane lipid rafts (Rinia et al. 2001; Zhuang et al. 2002). Furthermore, the flat areas also contained higher and irregular regions of various dimensions that sometimes appeared as ring-like

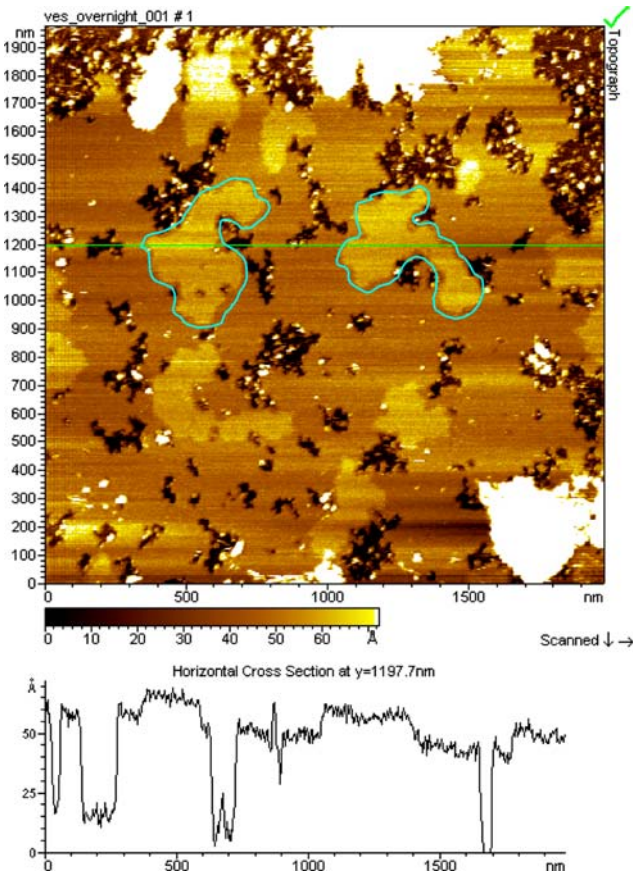

Fig. 3 Lipid domains in BBMs from *M. sexta*. Higher lipidic domains (delimited in *blue*) were sometimes observed within the membrane fragments. Their height is 5.1 ± 0.1 nm compared to that of the fragment themselves, i.e., 4.2 ± 0.1 nm. *Vertical profile along the green line* on the image is shown below

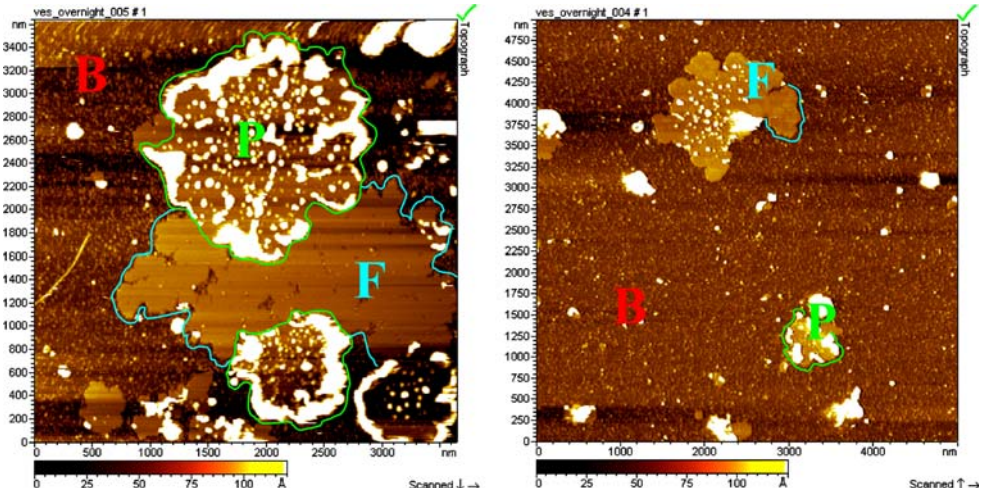

Fig. 2 Representative images of membrane fragments from *M. sexta* midgut BBMs. Most of the mica surface is covered by bumps (*B*) of various heights, which could possibly be unfused vesicles. The flat region is a membrane fragment (*F*, delimited in *blue*) with height of 4.2 ± 0.1 nm. Ring-like domains (*P*, delimited in *green*) were also observed, suggesting the presence of aggregates of membrane proteins

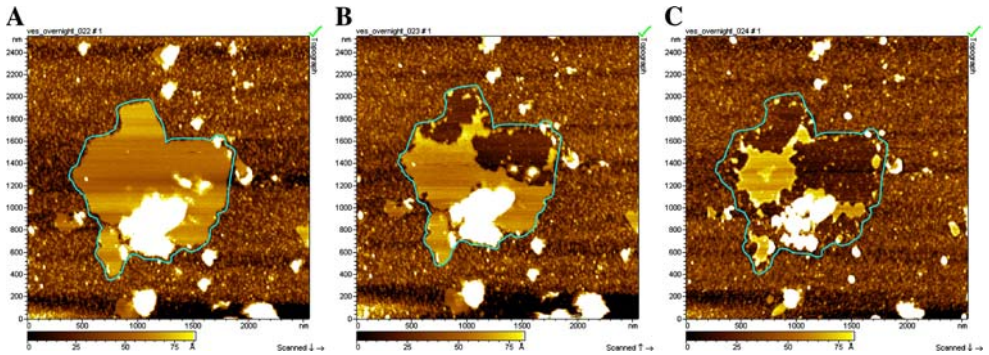

Fig. 4 Effect of PLA_2 on BBMs from *M. sexta*. Membrane fragments were gradually eroded by PLA_2 (5 μg/ml), demonstrating the essentially lipidic nature of the fragments. (**A**) Membrane fragment before addition of PLA_2 (delimited in *blue*). (**B**) Image of the same membrane fragment. PLA_2 was added when half of the image was scanned (scanning performed from bottom to top). The effect of PLA_2 was immediate, showing at the same time the efficacy of the solution exchange system. (**C**) Seven minutes after adding PLA_2, most of the membrane fragment was eroded

domains containing more of these higher structures, which may represent protein aggregates (Fig. 2). PLA_2 was used to confirm the lipidic nature of these flat areas. PLA_2 is an interfacially active, calcium-dependent enzyme which catalyzes cleavage of the *sn*-2 ester linkage of glycerophospholipids, yielding fatty acid and lysophospholipid (Six and Dennis 2000). Following the addition of PLA_2 (5 μg/ml), gradual erosion of the flat areas was observed (Fig. 4), in a way similar to that reported for phospholipid bilayers (Moraille and Badia 2005), demonstrating the essentially phospholipidic nature of the eroded areas. From the above, it appears that the flat areas originate from fragments of BBMV material deposited onto mica, with the smooth domains being bilayers of native lipid, the higher ones with longer chain lipids. These membrane fragments likely result from the fusion of BBM patches or BBMVs. On the other hand, the irregular regions are likely constituted by protein aggregates (Schillers et al. 2001; Fotiadis et al. 2004).

Imaging of Cry1 Toxins on *M. sexta* Midgut BBM Fragments

The presence of native membrane material and its receptors was expected to promote *Bt* toxin interaction with the membrane, thereby increasing the toxin density at the surface of the membrane, which should favor the observation of toxin molecules by AFM. After incubation with either 8 or 40 μg/ml of Cry1Aa, a toxin active against *M. sexta*, new structures were observed that were limited either to certain membrane fragments or to fragment regions (Fig. 5), suggesting specific interactions with these areas, likely through the toxin receptors or other specific membrane proteins or lipids. Similar results were obtained with two other toxins active against *M. sexta*, Cry1Ac and Cry1C, at the same doses as above. Such structures were never observed when identical protocols were conducted in the absence of toxin (control conditions). For Cry1Aa, Cry1Ac and Cry1C, the number of structures on the membrane fragments increased with incubation time and reached a plateau within 4 h (Figs. 6 and 7). In certain cases, a few of these structures were closely grouped together (Figs. 5B and 7, blue arrows), suggesting a cluster-like organization as reported elsewhere (Peyronnet et al. 2002). The heights of these structures over the membrane surface were 5.4 ± 0.2 nm for Cry1Aa ($n = 70$), 6.7 ± 0.2 nm for Cry1Ac ($n = 37$) and 5.1 ± 0.5 nm for Cry1C ($n = 8$) (Table 1). Their diameters were estimated to be 36.2 ± 0.8 nm for Cry1Aa ($n = 70$), 34.6 ± 1.5 nm for Cry1Ac ($n = 37$) and 39 ± 4 nm for Cry1C ($n = 8$) (Table 1). These dimensions did not depend on toxin concentration. Interestingly, these structures appear quite similar to those observed on DPPC-DOPC bilayers. This result can be set in parallel with the finding of similar pore sizes determined in functional assays on planar receptor-free lipid bilayers and on receptor-containing BBMVs (Peyronnet et al. 2002; Tran et al. 2001). Similarly, previous single ion channel measurements on planar lipid bilayers showed similar values of conductance in the presence or absence of purified toxin receptors (Schwartz et al. 1997b). Together, these findings strongly suggest that the general features of the pore architecture in the membrane are similar, whether the receptors are present or not. The AFM-measured values, when compared to X-ray crystallographic data of Cry1Aa (Grochulski et al. 1995) indicating that a single toxin molecule in solution measures $8.0 \times 5.5 \times 5.5$ nm, suggest that the observed structures contain most likely several toxin molecules, possibly with a large portion of each molecule lying on the membrane surface (Schwartz et al. 1997a; Masson et al. 1999). The oligomerization mechanism of Cry1 toxins is still largely unknown, and several schemes have been envisaged (Schwartz and Laprade 2000). For example, the toxin molecules could form an

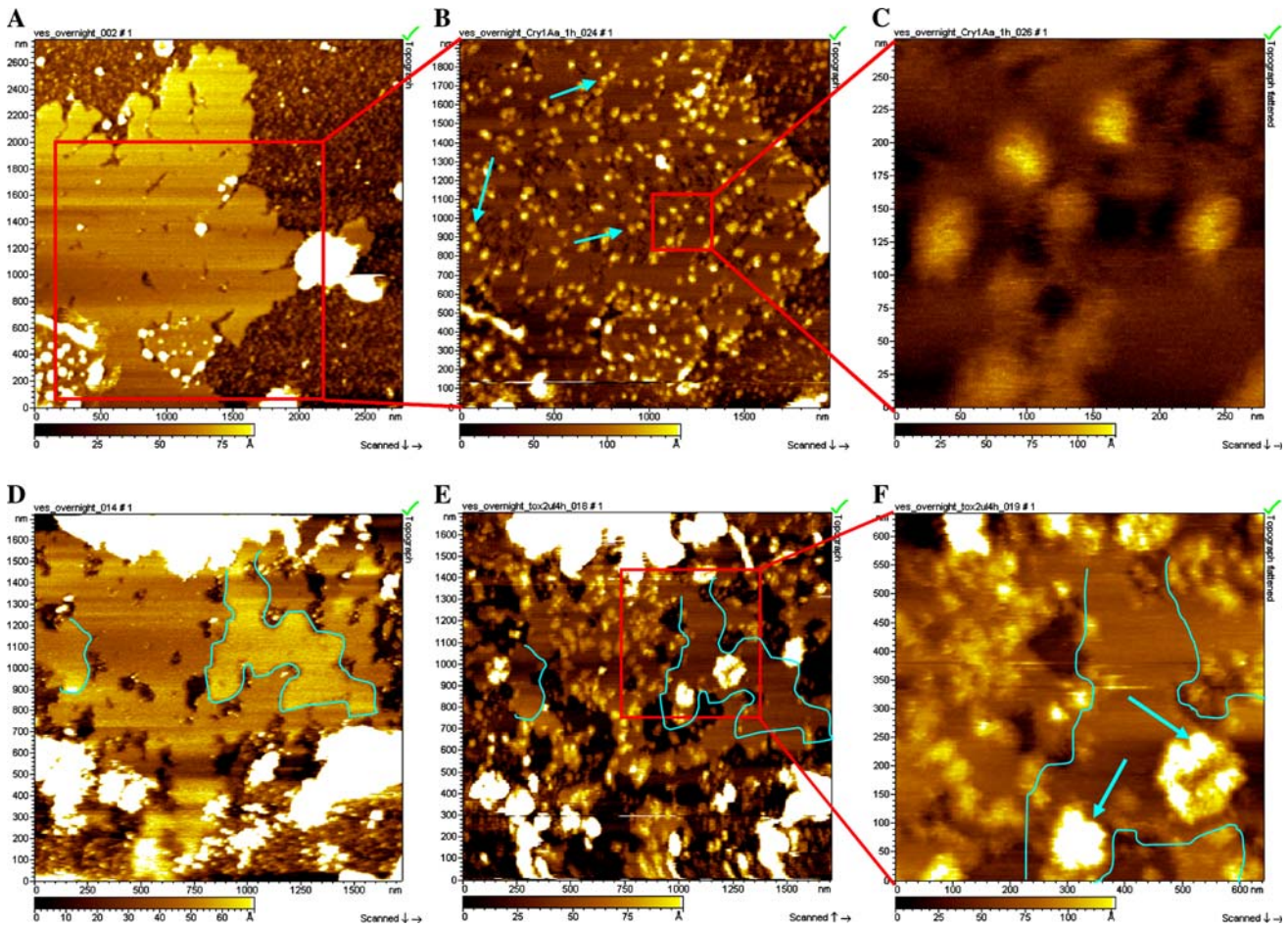

Fig. 5 Interaction of Cry1Aa toxin with BBMs from *M. sexta*. After incubation with Cry1Aa, structures were observed either on certain membrane fragments or on certain regions of the fragments. (**A**) Membrane fragment in the absence of toxin. (**B**) Same fragment after 1-h incubation with Cry1Aa at 40 μg/ml, showing toxin structures (approximately 35 nm in diameter and 5–7 nm high), more or less evenly distributed (40–60 toxin structures/μm^2) over the surface of the fragment. *Arrows* point to closely positioned structures. (**C**) Magnification (approximately x7) of the structures shown in (**B**). (**D**) Another membrane fragment showing a higher lipidic domain (delimited in *blue*) in the absence of toxin. (**E**) Same as (**D**), after 4-h incubation with Cry1Aa at 8 μg/ml. Toxin structures appeared mainly at the surface of the lower lipidic region. In the higher domains, virtually no such structures were observed. (**F**) Magnification (approximately ×3) of an area containing the two lipidic domains observed in (**E**). In addition, but very rarely, higher and larger aggregates of toxins could be seen on these higher domains (*blue arrows*)

oligomeric prepore either before or after docking onto a particular receptor (e.g., a cadherin in the case of Cry1Ab; Bravo et al. 2004). Alternatively, oligomerization may be a progressive process that takes place in the membrane, starting with a single toxin molecule binding to its receptor and inserting into the membrane, followed by the sequential addition of other toxin molecules. Such a process may well correspond to what is illustrated in Fig. 6, where the observed structures increased in size, up to about 35 nm in diameter, as a function of time.

In order to characterize the appearance of these structures on membrane fragments and attempt to identify and quantify differences in the way these toxins interact with their target membrane, our observations were divided into four categories (Table 2): (1) fragments that show no obvious structures; (2) fragments in which structures are observed mostly at their edges, i.e., either at the periphery of the fragments or at the edges of defects created by AFM tip erosion; (3) fragments in which structures are observed on both the surface and the borders of the fragments but with a clear preponderance for the surface; and (4) fragments in which structures form dense 2-D arrangements. Each experiment consisted of observations of the same fragments after 1 and 4 h of incubation with a single dose (either 8 or 40 μg/ml) of each toxin. For each toxin and each concentration, 10 membrane fragments were imaged. With Cry1Aa, after an incubation time of 1 h, one of the 10 observed membrane fragments showed structures distributed over most of the area at 8 μg/ml and two of them at 40 μg/ml (Table 2). At 40 μg/ml, incubating the toxin for 4 h did not increase the surface coverage, suggesting a saturating mechanism. On the other hand, larger toxin

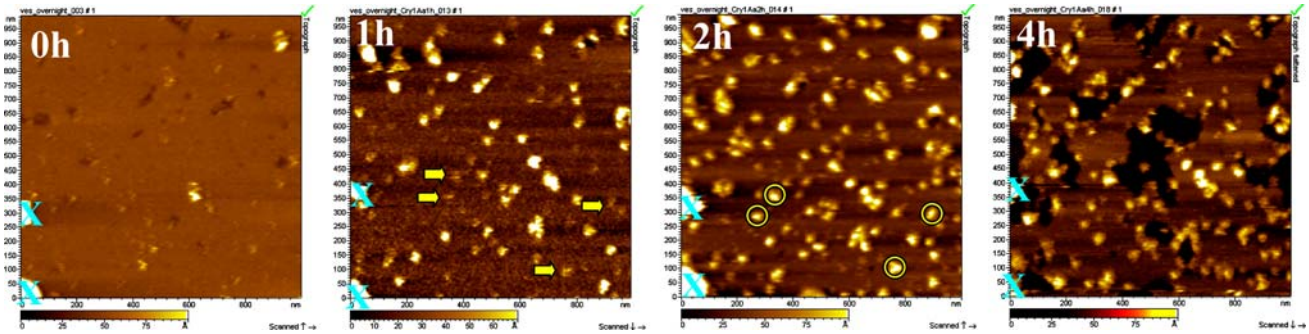

Fig. 6 Time course of Cry1Aa interaction with BBMs from *M. sexta*. The same area was imaged before and after a total of 1-, 2- and 4-h incubation with Cry1Aa (40 μg/ml). *Blue Xs* are reference markers. Small structures appeared after 1 h of toxin exposure (*yellow arrows*) that attained their maximum size of approximately 35 nm in diameter and a height of 5–7 nm after 2 h (*yellow circles*). After 4 h, the number of such structures reached a plateau and degradation of the membrane by the AFM tip was clearly observed and revealed the mica surface (*dark areas*)

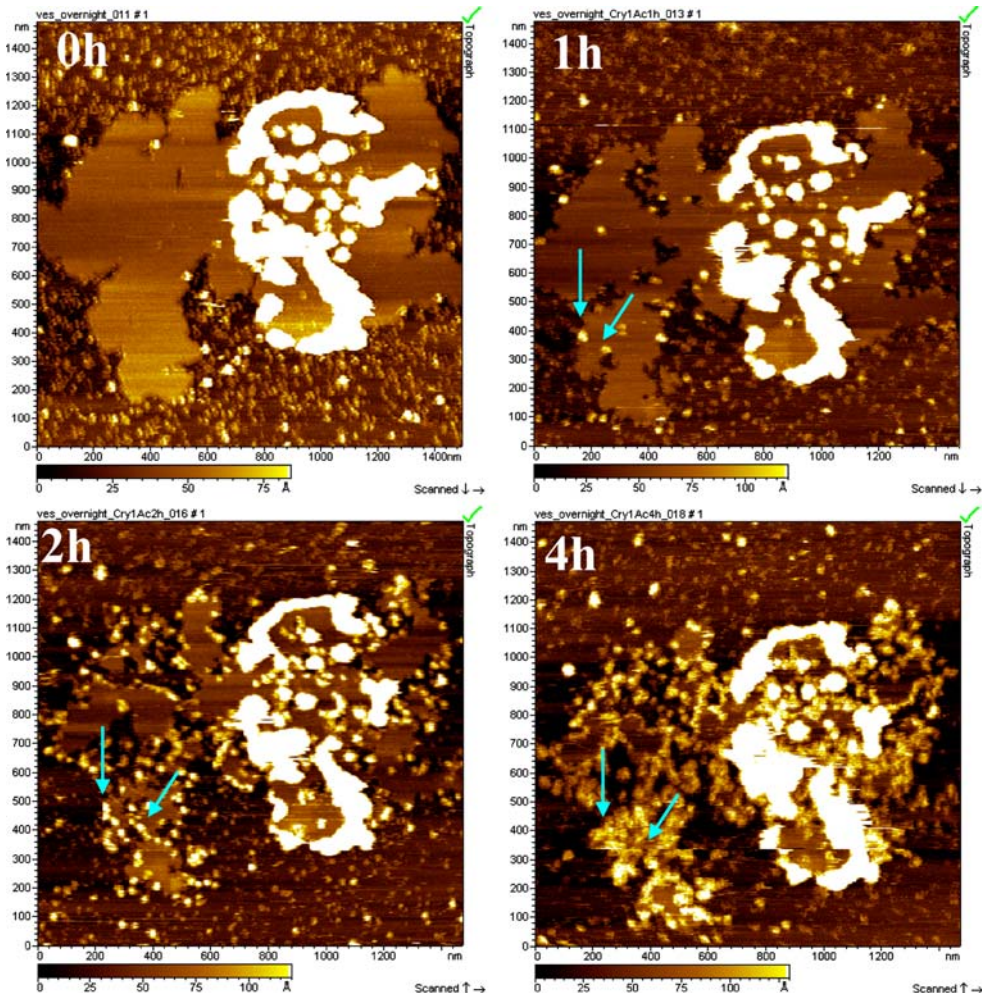

Fig. 7 Time course of Cry1Ac interaction with BBMs from *M. sexta*. The same area was imaged before and after a total of 1-, 2- and 4-h incubation with Cry1Ac (40 μg/ml). As shown by the *blue arrows*, a few toxins observed after 1 h in the defects of the membrane fragment generated pearl-like strings of toxin structures after 2 h, resulting in a dense 2-D arrangement after 4 h. Such arrangements were never observed with Cry1Aa (see Figs. 5 and 6)

concentrations and longer incubation times increased the probability of toxin insertion at the edges of the membrane fragments. The number of membrane fragments (out of 10) observed with the toxin mainly at their edges increased from zero after 1 h to five after 4 h at 8 μg/ml and from five after 1 h to eight after 4 h at 40 μg/ml. In situations such as those of Figs. 5 and 6, where good coverage of the fragment surface by the toxin structures was obtained (category 3 above), 89% presented a density of 40–60 structures/μm^2, which could represent an estimate of the

Table 1 Measured heights and diameters of Cry toxins interacting with membrane fragments: mean ± SEM

	Height (nm)	Diameter (nm)
Cry1Aa ($n = 70$)[a]	5.4 ± 0.2	36.2 ± 0.8
Cry1Ac ($n = 37$)[a]	6.7 ± 0.2	34.6 ± 1.5
Cry1C ($n = 8$)[a]	5.1 ± 0.5	39 ± 4
Cry1Ac 2-D arr. ($n = 5$)[a]	6.1 ± 0.3	N A

[a] n, number of toxin structures or dense 2-D arrangements that have been cross-sectioned

density of Cry1Aa *Bt* receptors in particular regions of the *M. sexta* midgut apical membrane.

In contrast to Cry1Aa, Cry1Ac did not form evenly distributed structures on the surface of the membrane fragments (Table 2). However, like Cry1Aa, Cry1Ac formed structures at the edges of the fragments, and its density and distribution depended on toxin concentration and incubation time (Table 2). Indeed, while at 8 μg/ml and after 1 h incubation virtually no structures were observed at the edges, three fragments out of 10 showed such structures after 4 h. At 40 μg/ml, five fragments out of 10 showed toxin structures at the edges after 1 h, similar to Cry1Aa. Also, in contrast to Cry1Aa, Cry1Ac at 40 μg/ml formed dense 2-D arrangements on one fragment out of 10 after 1 h and on seven fragments out of 10 after 4 h (Table 2, Figs. 7 and 8). The height of these 2-D arrangements was 6.1 ± 0.3 nm ($n = 5$), similar to that of the single structures formed by Cry1Ac (6.7 ± 0.2 nm, $n = 37$) (Table 1). It appears that the formation of these arrangements is initiated by a few isolated toxins, mostly located at the edges of the fragments, in a time- and dose-dependent manner, eventually reaching saturation (Fig. 7). Indeed, addition of more Cry1Ac toxin after formation of dense 2-D arrangements did not increase their size (not shown), suggesting a limited number of specific binding sites on the toxin structures and/or the membrane. Cry1Ac thus demonstrates a much higher level of toxin–toxin interaction than Cry1Aa.

With Cry1C, good surface coverage (category 3 above, Table 2) was never observed after 1 h, either at 8 or at 40 μg/ml. However, after 4 h, good coverage was observed on one out of 10 fragments with 8 μg/ml of the toxin and on two fragments out of 10 at 40 μg/ml (Fig. 9 and Table 2), similar to what was observed with Cry1Aa after 4 h (Figs. 5 and 6). Like Cry1Aa and Cry1Ac, Cry1C interacted with the membrane fragments at the edges but to a lesser extent. Indeed, the percentage of fragments showing Cry1C structures at their edges did not change (one out of 10) between 1 and 4 h of 8 μg/ml toxin exposure and increased slightly (from two fragments to three out of 10) between 1 and 4 h of exposure to 40 μg/ml Cry1C.

Cry1Aa toxin distribution in particular regions of some fragments (Fig. 5B, D–F) strongly suggests that its receptors are localized in these regions, although the latter could not be imaged in the absence of toxin, possibly because of their flexibility over the BBM, like that of

Table 2 Toxin structures interacting with membrane fragments: each experiment was conducted on the same membrane fragment after 1 and 4 h of incubation with the toxin

Toxin type (Cry)	Toxin dose[b] (μg/ml)	Incubation time (h)	Number of fragments with particular localization of structures			
			None[a]	Edges[a]	Surface[a]	2-D arrangement[a]
1Aa	8	1	9	0	1	0
		4	3	5	2	0
	40	1	3	5	2	0
		4	0	8	2	0
1Ac	8	1	10	0	0	0
		4	7	3	0	0
	40	1	4	5	0	1
		4	0	3	0	7
1C	8	1	9	1	0	0
		4	8	1	1	0
	40	1	8	2	0	0
		4	5	3	2	0

[a] The appearance of these structures on membrane fragments was divided into four categories: (1) number of fragments without structures (None), (2) number of fragments presenting structures mainly at edges (Edges), (3) Number of fragments presenting structures mainly on the surface (Surface) and (4) number of fragments presenting dense 2-D arrangement of structures (2-D arrangement). Each experiment consisted of observations of the same fragments after 1 and 4 h of incubation with a single dose (either 8 or 40 μg/ml) of each toxin

[b] For each toxin and each concentration, 10 membrane fragments were imaged

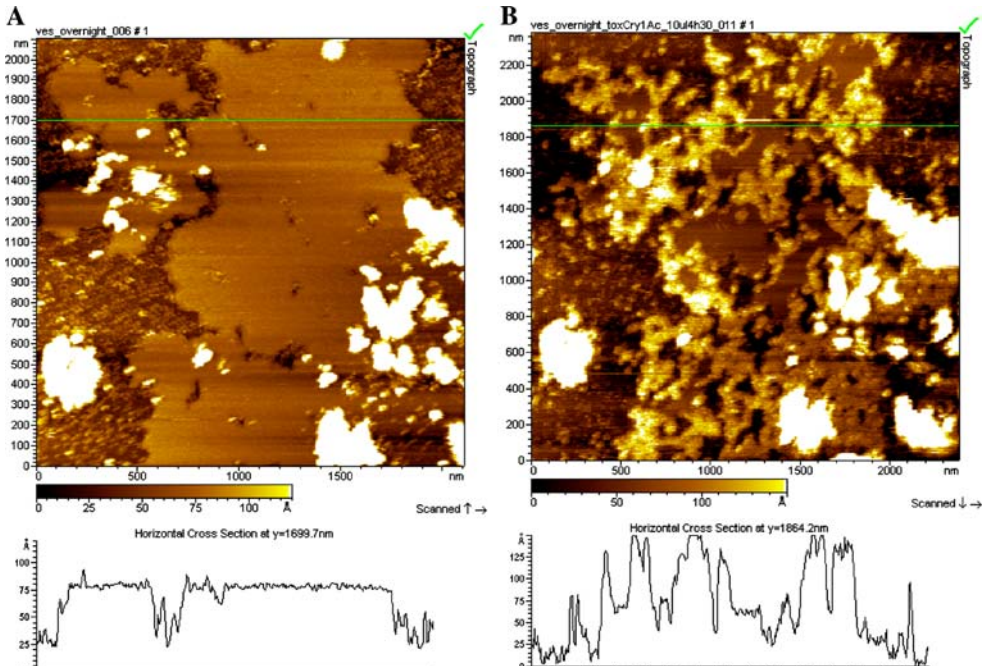

Fig. 8 Dense 2-D arrangements formed by Cry1Ac toxin interacting with BBMs from *M. sexta*. (**A**) Large membrane fragment before addition of toxin. (**B**) Same area after 4-h incubation with 40 µg/ml Cry1Ac. *Vertical profile along the green line* on the image is shown below

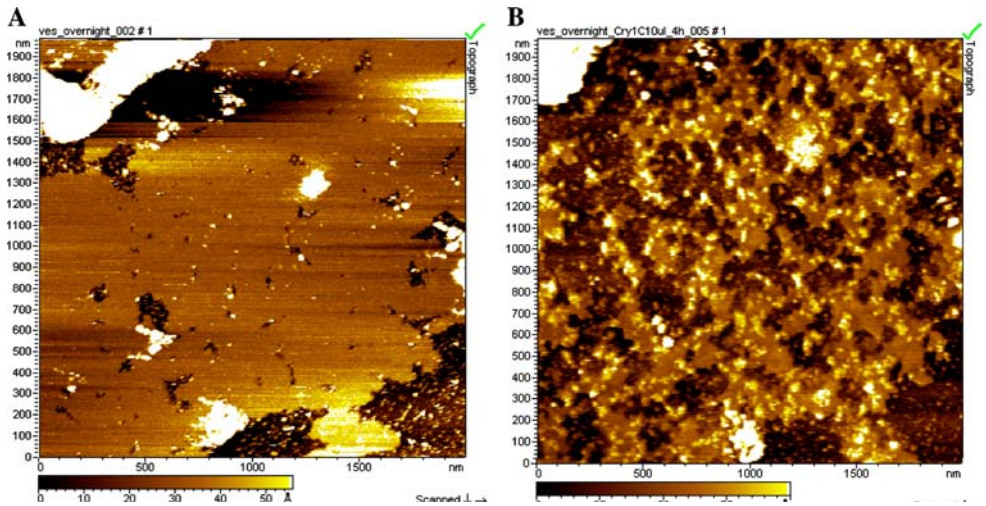

Fig. 9 Interaction of Cry1C toxin with BBMs from *M. sexta*. (**A**) Membrane fragment in the absence of toxin. (**B**) Same fragment after 4-h incubation with Cry1C at 8 µg/ml. Toxin structures were observed on the fragments, with similar dimensions and distribution to what was observed with Cry1Aa (see Figs. 5 and 6). Degradation of the membrane fragment by the AFM tip is clearly observed (*dark areas*)

GPI-anchored proteins (Ikezawa 2002). Indeed, most of these receptors are members of the APN, alkaline phosphatase or cadherin families, the two former types being attached to the membrane by a highly flexible GPI anchor and the latter possessing a single membrane-crossing region (Wheelock and Johnson 2003). On the other hand, certain membrane fragments were devoid of toxins (Table 2). It is possible that the imaged BBMs originated from different regions of the midgut, which would potentially affect the receptor type and density found in AFM samples. Furthermore, BBMV deposition on mica, followed by the formation of a single bilayer membrane, may not always result in the outside–out configuration in which receptors would be properly exposed to the bathing solution and, thus, to the toxins. Therefore, the number and availability of the receptors may be different under our AFM conditions from those found either in binding or light-scattering assays on BBMVs or in planar lipid bilayer experiments in which BBMVs were reconstituted. Nevertheless, our data clearly demonstrate that AFM images of BBMs in the presence of *Bt* toxins are dramatically different from those of BBMs alone and that the toxin interacts only with certain regions of the membrane fragments. This provides the first AFM evidence for the existence of specific interactions between *Bt* toxins and target insect midgut membranes.

Detergent-resistant microdomains of plasma membrane, or lipid rafts, have been proposed as a critical site in the mode of action of the *Bt* toxin Cry1Ab, i.e., the site of toxin preoligomer binding to APN and insertion into the gut membrane (Bravo et al. 2004). Such lipid rafts have been imaged by AFM in artificial lipid mixtures (Yuan et al. 2002; Milhiet et al. 2002; Giocondi et al. 2000), but their biological existence or relevance is still a matter of debate (Heerklotz 2002; Munro 2003). Detailed analysis of lipids bound to APN from *M. sexta* BBM, which act as receptors of Cry1Ac and Cry1C toxins, revealed that long, unsaturated-chain free fatty acids and diacylglycerol were involved (Sangadala et al. 2001) while detergent-insoluble lipids extracted from *M. sexta* and *Heliothis virescens* midgut BBMV showed a large amount of cholesterol and sphingomyelin (Zhuang et al. 2002). Such a mixture of lipids may also be present in our AFM samples and explain the different domains that were observed, some differing in height by about 1 nm. In our experiments, however, the higher lipidic domains seemed to be largely deprived of the toxin structures (Fig. 5D–F), suggesting that the toxin receptors are localized in the lower domains. The *Bt* toxin molecules may actually be considered as reporters of the presence on the BBM of the *Bt* receptors to which they bind. Our data suggest therefore that these receptors are localized in the lower areas of the lipid surface and that their distribution depends on the receptor–toxin pair under consideration.

Toxin Dose

Interestingly, while Cry1Aa, Cry1Ac, Cry1Ba and Cry1C toxins have been shown to form ion channels in receptor-free planar lipid bilayers at 5–10 μg/ml doses, much lower toxin concentrations were required either when a *Bt* receptor complex from *M. sexta* was reconstituted in the membranes (20–100 ng/ml Cry1Ac; Schwartz et al. 1997b) or when *Lymantria dispar* (gypsy moth, Lepidoptera) BBMVs were fused to the bilayers (60–80 ng/ml Cry1Aa; Peyronnet et al. 2001). In the former case, native lipids were associated with the receptor (Sangadala et al. 2001); and in the latter case, the planar lipid bilayers were enriched with several *Bt* receptors and other membrane proteins in addition to native lipids, including possibly some structural proteins (Terra et al. 2006; Kirouac et al. 2006). In the present AFM study, rather high doses (8 and 40 μg/ml, i.e., in the range of those used in receptor-free planar lipid bilayer experiments) were required to observe the interaction between *Bt* toxins and BBMs. In addition, the time course of these interactions was considerably longer than that needed for pore formation in membrane vesicles (Fortier et al. 2005, 2007; Vachon et al. 2004). This may be related to the difference in sensitivity of the methods. Indeed, permeability measurements are very sensitive, whereas in AFM a certain number of structures must be present on a given surface to allow the observer to identify their presence with a reasonable level of certainty. Alternatively, this may result from the fact that the fluidity of the membrane was reduced due to the vicinity of the mica substrate, thus reducing the probability of insertion of the toxin (Stottrup et al. 2004). It could also be due to long-range repulsive electrostatic forces exerted by the negatively charged mica. These would be significant at the low ionic strength used in the present experiments, which is that used in permeability essays (Fortier et al. 2005; Müller et al. 1999). The need for high doses may be related also to a lower accessibility of the receptors at the sample surface.

Toxin Specificity

To verify the specificity of the interactions of Cry1Aa, Cry1Ac and Cry1C with the membrane fragments, Cry1Ba, a toxin that is inactive against *M. sexta*, was tested. At the maximum concentration and incubation time used, no structures were observed on nine of the 10 membrane fragments. Moreover, when observed, the structures were sparse and located at the edge of the lipid areas and in defects of the membrane fragments (not shown). The fact that Cry1Ba, for which there is no receptor in *M. sexta* midgut (Höfte and Whiteley 1989), could only be observed at edges and defect sites under maximum concentration and incubation time seems to indicate that this protein interacted directly with the lipids, similar to what has been observed electrophysiologically in planar lipid bilayers (Schwartz et al. 1997b).

The relation between the *Bt* toxin deposition patterns observed on the AFM images and the localization of their receptors on the midgut apical membrane may be relevant to the in vivo specificity of *Bt* toxins. The fact that the Cry1Aa and Cry1C receptors are likely to be more numerous in BBMs than the Cry1Ac receptors (Höfte and Whiteley 1989; Höfte et al. 1988; Van Rie et al. 1989, 1990) could explain the evenly distributed patterns observed with the two former toxins and their absence with the latter. Indeed, good surface coverage was attained with Cry1Aa and Cry1C. Interestingly, Cry1Ac was the only one of the three toxins that formed dense 2-D surface arrangements, which may be related to the higher toxicity of this protein (reviewed in Tran et al. 2001). For this protein, favorable conformation changes may have promoted toxin–toxin interaction of free toxin molecules, either with those inserted at the edges of membrane fragments, which would explain the way these 2-D arrangements developed from the fragment edges, or with other toxin molecules bound to their receptors, resulting in the dense 2-D arrangements observed. Finally, the observation of the various toxins, including Cry1Ba, at the

edges of the membrane fragments, is likely related to facilitated toxin–lipid interaction in membrane default areas. These are known to promote protein–lipid interactions (Puntheeranurak et al. 2005). Taken together, these observations strongly suggest that Cry1Aa, Cry1Ac and Cry1C interactions with the membrane fragments are specific and most likely mediated through membrane receptors and toxin–toxin interactions. However, the different patterns of interaction of these three toxins with the membrane suggest that they associate with different receptor molecules or toxin regions.

Conclusion

This study provides the first visualization of the interaction between *Bt* toxins and BBMs derived from midgut cells of *M. sexta* larvae. These membranes are the natural targets of *Bt* toxins, which have been shown to bind to specific receptors located on their surface and, in a subsequent step, to form pores and permeabilize the membranes, leading to cell swelling and lysis. AFM measurements established that Cry1Aa, Cry1Ac and Cry1C proteins, three closely related toxins active against *M. sexta*, formed structures approximately 35 nm in diameter and 5.1–6.7 nm in height after exposure of the BBMs to the toxins. The three toxins did not interact in the same way with the BBM, in terms of either kinetics or localization and assembly. In addition to toxin–toxin and toxin–lipid interactions, these structures, in regions where they are evenly distributed, appear to be formed largely through toxin–receptor interactions, thus possibly making the toxin molecules the reporters of their receptors and therefore providing an indirect way to visualize both the location and density of these receptors on the BBM. Our data therefore suggest that these receptors are localized in the thinner regions of the lipid surface observed by AFM and that their distribution depends on the receptor–toxin pair under consideration. Finally, the dimensions and distribution of the toxins imaged by AFM on natural midgut membrane may well reflect those of the functional pores formed by *Bt* proteins in vivo.

Acknowledgements We thank Stéphanie Juneau (Department of Astronomy, University of Arizona, Tucson, AZ), who initiated the project as a research trainee; Patricia Moraille and Jacqueline Sanchez (Department of Chemistry, Université de Montréal, Montréal, Canada) for technical advice on AFM; and Lucie Marceau, Marc Juteau and Mireille Marsolais (Groupe d'étude des protéines membranaires, Université de Montréal) for producing the purified *Bt* toxins and for other technical support. We are indebted to Frédéric Girard, Martin Kirouac and Vincent Vachon for stimulating discussions. E. L. was supported by a scholarship from the Fonds de la recherche en santé du Québec. This work was supported by grants from the Natural Sciences and Engineering Research Council of Canada and from the Fonds québécois de recherche sur la nature et les technologies.

References

Bravo A, Gómez I, Conde J, Muñoz-Garay C, Sánchez J, Miranda R, Zhuang M, Gill SS, Soberón M (2004) Oligomerization triggers binding of a *Bacillus thuringiensis* Cry1Ab pore-forming toxin to aminopeptidase N receptor leading to insertion into membrane microdomains. Biochim Biophys Acta 1667:38–46

Chen Y, Cai JY, Zhao T, Wang CX, Dong S, Luo SQ, Chen ZW (2005) Atomic force microscopy imaging and 3-D reconstructions of serial thin sections of a single cell and its interior structures. Ultramicroscopy 103:173–182

Danker T, Mazzanti M, Tonini R, Rakowska A, Oberleithner H (1997) Using atomic force microscopy to investigate patch-clamped nuclear membrane. Cell Biol Int 21:747–757

El Kirat K, Burton I, Duprès V, Dufrêne YF (2005) Sample preparation procedures for biological atomic force microscopy. J Microsc 218:199–207

Fortier M, Vachon V, Kirouac M, Schwartz JL, Laprade R (2005) Differential effects of ionic strength, divalent cations and pH on the pore-forming activity of *Bacillus thuringiensis* insecticidal toxins. J Membr Biol 208:77–87

Fortier M, Vachon V, Marceau L, Schwartz JL, Laprade R (2007) Kinetics of pore formation by the *Bacillus thuringiensis* toxin Cry1Ac. Biochim Biophys Acta 1768:1291–1298

Fotiadis D, Liang Y, Filipek S, Saperstein DA, Engel A, Palczewski K (2004) The G protein–coupled receptor rhodopsin in the native membrane. FEBS Lett 564:281–288

Gill SS, Cowles EA, Pietrantonio PV (1992) The mode of action of *Bacillus thuringiensis* endotoxins. Annu Rev Entomol 37:615–636

Giocondi MC, Vié V, Lesniewska E, Goudonnet JP, Le Grimellec C (2000) In situ imaging of detergent-resistant membranes by atomic force microscopy. J Struct Biol 131:38–43

Grochulski P, Masson L, Borisova S, Pusztai-Carey M, Schwartz JL, Brousseau R, Cygler M (1995) *Bacillus thuringiensis* CrylA(a) insecticidal toxin: crystal structure and channel formation. J Mol Biol 254:447–464

Heerklotz H (2002) Triton promotes domain formation in lipid raft mixtures. Biophys J 83:2693–2701

Hodgman TC, Ellar DJ (1990) Models for the structure and function of the *Bacillus thuringiensis* δ-endotoxins determined by compilational analysis. DNA Seq 1:97–106

Höfte H, Whiteley HR (1989) Insecticidal crystal proteins of *Bacillus thuringiensis*. Microbiol Rev 53:242–255

Höfte H, Van Rie J, Jansens S, Van Houtven A, Vanderbruggen H, Vaeck M (1988) Monoclonal antibody analysis and insecticidal spectrum of three types of lepidopteran-specific insecticidal crystal proteins of *Bacillus thuringiensis*. Appl Environ Microbiol 54:2010–2017

Ikezawa H (2002) Glycosylphosphatidylinositol (Gpi)-anchored proteins. Biol Pharm Bull 25:409–417

Janovjak H, Kedrov A, Cisneros DA, Sapra KT, Struckmeier J, Muller DJ (2006) Imaging and detecting molecular interactions of single transmembrane proteins. Neurobiol Aging 27:546–561

Kirouac M, Vachon V, Fortier M, Trudel MC, Berteloot A, Schwartz JL, Laprade R (2006) A mechanical force contributes to the "osmotic swelling'' of brush-border membrane vesicles. Biophys J 91:3301–3312

Knowles BJ, Ellar DJ (1987) Colloid-osmotic lysis is a general feature of the mechanism of action of *Bacillus thuringiensis* delta-endotoxin with different insect specificity. Biochim Biophys Acta 924:509–518

Li J, Carroll J, Ellar DJ (1991) Crystal structure of insecticidal δ-endotoxin from *Bacillus thuringiensis* at 2.5 Å resolution. Nature 353:815–821

Markiewicz P, Goh MC (1994) Atomic force microscopy probe tip visualization and improvement of images using a simple deconvolution procedure. Langmuir 10:5–7

Masson L, Préfontaine G, Péloquin L, Lau PCK, Brousseau R (1989) Comparative analysis of the individual protoxin components in P1 crystals of *Bacillus thuringiensis* subsp. kurstaki isolates NRD-12 and HD-1. Biochem J 269:507–512

Masson L, Mazza A, Gringorten L, Baines D, Aneliunas V, Brousseau R (1994) Specificity domain localization of *Bacillus thuringiensis* insecticidal toxins is highly dependent on the bioassay system. Mol Microbiol 14:851–860

Masson L, Tabashnik BE, Liu YB, Brousseau R, Schwartz JL (1999) Helix 4 of the *Bacillus thuringiensis* Cry1Aa toxin lines the lumen of the ion channel. J Biol Chem 274:31996–32000

Milhiet PE, Vié V, Giocondi MC, Le Grimellec C (2001) AFM characterization of model rafts in supported bilayers. Single Molecules 2:109–112

Milhiet PE, Giocondi MC, Baghdadi O, Ronzon F, Roux B, Le Grimellec C (2002) Spontaneous insertion and partitioning of alkaline phosphatase into model lipid rafts. EMBO Rep 3:485–490

Milhiet PE, Gubellini F, Berquand A, Dosset P, Rigaud JL, Le Grimellec C, Lévy D (2006) High-resolution AFM of membrane proteins directly incorporated at high density in planar lipid bilayer. Biophys J 91:3268–3275

Moraille P, Badia A (2005) Enzymatic lithography of phospholipid bilayer films by stereoselective hydrolysis. J Am Chem Soc 127:6546–6547

Müller DJ, Fotiadis D, Scheuring S, Müller SA, Engel A (1999) Electrostatically balanced subnanometer imaging of biological specimens by atomic force microscopy. Biophys J 76:1101–1111

Müller DJ, Heymann JB, Oesterhelt F, Möller C, Gaub H, Büldt G, Engel A (2000) Atomic force microscopy of native purple membrane. Biochim Biophys Acta 1460:27–38

Munro S (2003) Lipid rafts: elusive or illusive? Cell 115:377–388

Peyronnet O, Vachon V, Schwartz JL, Laprade R (2001) Ion channels induced in planar lipid bilayers by the *Bacillus thuringiensis* toxin Cry1Aa in the presence of gypsy moth (*Lymantria dispar*) brush border membrane. J Membr Biol 184:45–54

Peyronnet O, Nieman B, Généreux F, Vachon V, Laprade R, Schwartz JL (2002) Estimation of the radius of the pores formed by the *Bacillus thuringiensis* Cry1C δ-endotoxin in planar lipid bilayers. Biochim Biophys Acta 1567:113–122

Puntheeranurak T, Stroh C, Zhu R, Angsuthanasombat C, Hinterdorfer P (2005) Structure and distribution of the *Bacillus thuringiensis* Cry4Ba toxin in lipid membranes. Ultramicroscopy 105:115–124

Rinia H, Snel M, van der Eerden J, de Kruijff B (2001) Visualizing detergent resistant domains in model membranes with atomic force microscopy. FEBS Lett 501:92–96

Sangadala S, Azadi P, Carlson R, Adang MJ (2001) Carbohydrate analyses of *Manduca sexta* aminopeptidase N, co-purifying neutral lipids and their functional interactions with *Bacillus thuringiensis* Cry1Ac toxin. Insect Biochem Mol Biol 32:97–107

Schillers H, Danker T, Madeja M, Oberleithner H (2001) Plasma membrane protein clusters appear in CFTB-expressing *Xenopus laevis* oocytes after cAMP stimulation. J Membr Biol 180:205–212

Schnepf E, Crickmore N, Van Rie J, Lereclus D, Baum J, Feitelson J, Zeigler DR, Dean DH (1998) *Bacillus thuringiensis* and its pesticidal crystal proteins. Microbiol Mol Biol Rev 62:775–806

Schwartz JL, Garneau L, Savaria D, Masson L, Brousseau R, Rousseau E (1993) Lepidopteran-specific crystal toxins from *Bacillus thuringiensis* form cation- and anion-selective channels in planar lipid bilayers. J Membr Biol 132:53–62

Schwartz JL, Juteau M, Grochulski P, Cygler M, Préfontaine G, Brousseau R, Masson L (1997a) Restriction of intramolecular movements within the Cry1Aa toxin molecule of *Bacillus thuringiensis* through disulfide bond engineering. FEBS Lett 410:397–402

Schwartz JL, Lu YJ, Söhnlein P, Brousseau R, Laprade R, Masson L, Adang MJ (1997b) Ion channels formed in planar lipid bilayers by *Bacillus thuringiensis* toxins in the presence of *Manduca sexta* midgut receptors. FEBS Lett 412:270–276

Schwartz JL, Laprade R (2000) Membrane permeabilisation by *Bacillus thuringiensis* toxins: protein insertion and pore formation. In: Charles JF, Delécluse A, Nielsen-LeRoux C (eds) Entomopathogenic bacteria: from laboratory to field application. Kluwer, Norwell, MA, pp 199–218

Six DA, Dennis EA (2000) The expanding superfamily of phospholipase A_2 enzymes: classification and characterization. Biochim Biophys Acta 1488:1–19

Stottrup BL, Veatch SL, Keller SL (2004) Nonequilibrium behavior in supported lipid membranes containing cholesterol. Biophys J 86:2942–2950

Terra WR, Costa RH, Ferreira C (2006) Plasma membranes from insect midgut cells. An Acad Bras Cienc 78:255–269

Tran LB, Vachon V, Schwartz JL, Laprade R (2001) Differential effects of pH on the pore-forming properties of *Bacillus thuringiensis* insecticidal crystal toxins. Appl Environ Microbiol 67:4488–4494

Vachon V, Préfontaine G, Rang C, Coux F, Juteau M, Schwartz JL, Brousseau R, Frutos R, Laprade R, Masson L (2004) Helix 4 mutants of the *Bacillus thuringiensis* insecticidal toxin Cry1Aa display altered pore-forming abilities. Appl Environ Microbiol 70:6123–6130

Van Rie J, Jansens S, Höfte H, Degheele D, Van Mellaert H (1989) Specificity of *Bacillus thuringiensis* δ-endotoxins—importance of specific receptors on the brush border membrane of the midgut of target insects. Eur J Biochem 186:239–247

Van Rie J, Jansens S, Höfte H, Degheele D, Van Mellaert H (1990) Receptors on the brush border membrane of the insect midgut as determinants of the specificity of *Bacillus thuringiensis* delta-endotoxins. Appl Environ Microbiol 56:1378–1385

Vié V, Van Mau N, Pomarède P, Dance C, Schwartz JL, Laprade R, Frutos R, Rang C, Masson L, Heitz F, Le Grimellec C (2001) Lipid-induced pore formation of the *Bacillus thuringiensis* Cry1Aa insecticidal toxin. J Membr Biol 180:195–203

Whalon ME, Wingerd BA (2003) *Bt*: mode of action and use. Arch Insect Biochem Physiol 54:200–211

Wheelock MJ, Johnson KR (2003) Cadherin-mediated cellular signaling. Curr Opin Cell Biol 15:509–514

Wielert-Badt S, Hinterdorfer P, Gruber HJ, Lin JT, Badt D, Wimmer B, Schindler H, Kinne RKH (2002) Single molecule recognition of protein binding epitopes in brush border membranes by force microscopy. Biophys J 82:2767–2774

Wolfersberger M, Luethy P, Maurer A, Parenti P, Sacchi VF, Giordana B, Hanozet GM (1987) Preparation and partial characterization of amino acid transporting brush border membrane vesicles from the larval midgut of the cabbage butterfly (*Pieris brassicae*). Comp Biochem Physiol 86A:301–308

Yuan CB, Furlong J, Burgos P, Johnston LJ (2002) The size of lipid rafts: an atomic force microscopy study of ganglioside GM_1 domains in sphingomyelin/DOPC/cholesterol membranes. Biophys J 82:2526–2535

Zhuang MB, Oltean DI, Gómez I, Pullikuth AK, Soberón M, Bravo A, Gill SS (2002) *Heliothis virescens* and *Manduca sexta* lipid rafts are involved in cry1A toxin binding to the midgut epithelium and subsequent pore formation. J Biol Chem 277:13863–13872